Approximate Low Dimensional Models based on Proper Orthogonal Decomposition for Black-Box Applications.

S. Ali[1], M. Damodaran[2], and K.E. Willcox[3]

[1] Department of Mathematics and Science, Singapore Polytechnic,
[2] School of Mechanical and Aerospace Engineering, Nanyang Technological University,
[3] Department of Aeronautics and Astronautics, Massachusetts Institute of Technology

***Abstract* — Many industrial applications in engineering and science are solved using commercial engineering solvers that function as black-box simulation tools. Besides being time consuming and computationally expensive, the actual mathematical models and underlying structure of these problems are for most part unknown. This paper presents a method for constructing approximate low-dimensional models for such problems using the proper orthogonal decomposition (POD) technique. We consider a heat diffusion problem and a contamination transport problem, where the actual mathematical models are assumed to be unknown but numerical data in time are available so as to enable the formation of an ensemble of snapshots The POD technique is then used to produce a set of basis functions that spans the snapshot collection corresponding to each problem. The key idea is then to assume some functional form of the low-order model, and use the available snapshot data to perform a least squares fit in the POD basis coordinate system to determine the unknown model coefficients. Initial results based on this approximation method seem to hold some promise in creating a predictive low-order model, that is, one able to predict solutions not included in the original snapshot set. Some issues arising from this approximation method are also discussed in this paper.**

***Index Terms* — linear system, proper orthogonal decomposition, black-box applications**

I. Introduction

Industrial design applications in engineering and science are often multidisciplinary, with large, complex structures. High performance computing abilities are able to solve these large scales and complex applications but the solutions of these problems are likely to be time consuming and computationally expensive for routine design applications. Therefore, an optimal use of such models in routine design work would benefit from low-order models [1]- [8] which are less time consuming, require much less computational effort, and yet, are able to capture the richness of the high-fidelity solutions.

Existing techniques to derive low-order models require a priori knowledge of the structure of the high-fidelity problem to be approximated. Since these problems are usually solved using commercial software that acts like a black box, in many cases the users have no knowledge of the process by which the results or solutions are obtained. In such cases, it is difficult to obtain low-order models using existing model reduction methods, which typically employ a Galerkin projection technique that necessitates knowledge of the underlying mathematical model. Ly and Tran [10] proposed a different technique of obtaining low-order models by combining the use of proper orthogonal decomposition (POD) and interpolation techniques. They have successfully demonstrated the capability of this technique on several problems where the mathematical models are assumed to be unknown. However, the limitation of interpolation techniques lies in the inability to extrapolate to ranges beyond the data provided; hence, interpolation cannot generally be applied to transient problems for which the low-order models are likely to be used to predict the solutions at times beyond the range of the available experimental or simulated data.

The aim of this work is to develop a method for constructing low-order models for dynamical systems that requires minimal prior knowledge of the higher dimensional or mathematical models of the problems. Similar to Caraballo et. al. [11] who designed a linear-quadratic optimal controller by fitting the estimators to the time coefficients obtained from the PIV images, the method uses POD to obtain the basis functions for the low-order model and fits the given data with an approximate model. Two application problems, namely a heat conduction problem and a contaminant transport problem are used to illustrate the method in this paper. The mathematical models of these application problems are assumed to be unknown and only their high-fidelity data are assumed known.

An overview of the method is presented in Section II. The two test applications problems and the results of the black-box modeling methodology are discussed in Section III. Section IV concludes with key observations gained

Manuscript received November 20, 2006. This work was supported in part by the Singapore-MIT Alliance Computational Engineering IUP.

S. Ali was with Nanyang Technological University, Singapore. She is now with the Department of Mathematics and Science, Singapore Polytechnic, 500 Dover Rd, Singapore (Tel: (65)-6870-4688; e-mail: shidrati@sp.edu.sg).

M. Damodaran is with the School of Mechanical and Aerospace Engineering, Nanyang Technological University (e-mail: mdamodaran@ntu.edu.sg).

K. Willcox is with the Department of Aeronautics and Astronautics, Massachusetts Institute of Technology (e-mail: kwillcox@mit.edu).

from this exercise.

II. Approximate Low-Order Model Using Proper Orthogonal Decomposition

Many model reduction methods employ a projection approach, which requires computation of a reduced-space basis. There are several methods of constructing the basis functions, including the reduced basis method [1]-[3], Krylov subspace methods [4]-[6] and the POD method [7]-[9]. In the case of the POD, the basis functions are derived from an ensemble of data obtained either through experiments or from a high-fidelity computational solver. The POD method is chosen in this paper since the basis vectors can be computed without any prior knowledge of the process that generates the data, i.e. the high-fidelity solver could be a black-box simulation system.

A. Proper orthogonal decomposition

The method of snapshots is used in this paper to construct the POD modes [8]. In this method, the POD modes are expressed as a linear combination of the "snapshots" of state variables of the high-fidelity or experimental system.

We consider a high-fidelity computational model with state variables contained in the vector $U(\vec{x},t)$, which has dimension n. The ensemble of snapshots in time can be expressed as $\{U(\vec{x},t_i)\in\Re^n, i=1,\ldots,M\}$, where M is the number of snapshots. Each POD mode can be expressed as linear combination of the snapshots, i.e.

$$\phi_j = \sum_{i=1}^{M} \beta_j^i U_i \tag{1}$$

where ϕ_j is the jth POD mode and $U_i = U(\vec{x},t_i)$ denotes the ith snapshot. It can be shown [12] that the set of coefficients, β_j =[β_j^1 , β_j^2 ,…, β_j^M], satisfies the eigenproblem

$$R\beta_j = \lambda_j \beta_j \tag{2}$$

where $R_{i,j} = (1/M)(U_i, U_j)$ and $(\cdot,\cdot)$ denotes an inner product. The *j*th eigenvalue of *R*, λ_j , determines the importance of the jth POD mode. The relative "energy" (in the 2-norm sense) of POD mode *i* is given by $\lambda_i / \sum_{j=1}^{M} \lambda_j$, and is often used as a criterion for selecting N, the number of basis functions to retain in the low-order model. Then the *N*th-order POD approximation of the state $U(\vec{x},t_k)$ can be expressed as

$$U_N(\vec{x},t_k) = \sum_{i=1}^{N} \alpha_i(t_k)\phi_i(\vec{x}) \tag{3}$$

for some $N < M$, where the coefficient $\alpha_i(t_k)$ gives the contribution of the ith POD mode.

B. Approximate low-order models

We consider a general application for which the state evolution

$$\dot{U} = X(U) \tag{4}$$

is described by a spatial differential operator, X , whose form is unknown. We desire to construct a low-order model of this system. Our first step is to assume a form of the low-order model, for example, we assume that the dynamical system described by (4) can be approximated by a linear, quadratic, or higher-order system of equations. For example, a linear approximation of (4) could be expressed as

$$\dot{U} = A + B\cdot U \tag{5}$$

and a quadratic approximation could be expressed as

$$\dot{U} = A + B\cdot U + U^T\cdot(C\cdot U). \tag{6}$$

where *A*, *B*, and *C* are respectively a vector, matrix, and tensor of appropriate dimension.

Projection of the approximate linear system described by (5) on the subspace spanned by the POD basis functions leads to the low-order model

$$\frac{d\alpha_i}{dt} = a_i + \sum_{j=1}^{N} b_{ij}\alpha_j \text{ , i=1,…N} \tag{7}$$

where the coefficients are given by

$$a_i = \sum_{j=1}^{n} \phi_{ij} A_j \text{ , i=1,…N} \tag{8}$$

and

$$b_{ij} = \sum_{l=1}^{n}\sum_{k=1}^{n} \phi_{ik} B_{kl} \phi_{lj} \text{ i=1,…N, j=1,…N} \tag{9}$$

Here, A_j denotes the *j*th component of the vector A, B_{kl} denotes the component in the *k*th row and *l*th column of the matrix B, and ϕ_{ij} denotes the *i*th component of the *j*th POD basis vector.

Similarly, in the quadratic case, the low-order model has the form

$$\frac{d\alpha_i}{dt} = a_i + \sum_{j=1}^{N} b_{ij}\alpha_j + \sum_{k=1}^{N}\sum_{j=1}^{N} c_{ijk}\alpha_j\alpha_k \text{ ,} \tag{10}$$

where a_i and b_{ij} are defined as in (8) and (9), and

$$c_{ijk} = \sum_{m=1}^{n}\sum_{l=1}^{n}\sum_{h=1}^{n} \phi_{ih}\phi_{jl}C_{hlm}\phi_{mk} \text{ .} \tag{11}$$

We note that the components of the low-order matrices and vectors expressed by a_i , b_{ij} , and c_{ijk} are analogous to those that would be obtained if a standard Galerkin projection were applied to a linear or quadratic high-fidelity model. However, in our black-box case, the approximate matrices and vectors given by A , B , and C are unknown, and therefore the elements of the matrices and vectors of the low-order model, a_i , b_{ij} , and c_{ijk} , are also unknown.

The key idea of this paper is that in order to construct the low-order model, the coefficients a_i , b_{ij} , and c_{ijk} can be

computed using simulation data combined with a least squares minimization technique [13]. Specifically, each POD modal coefficient, α_i , for all *N* coefficients, corresponding to the ensemble of snapshots are easily computed as

$$\alpha_i(t_k) = (\phi_i, U(\bar{x}, t_k)), \quad \text{k = 1,…,M} \qquad (12)$$

Similarly, the time derivatives of the POD modal coefficients for that same ensemble data, $\frac{d\alpha_i}{dt}$, can be computed by applying the finite difference method to the known values of α_i . For example, using a first-order forward Euler time-stepping scheme, we can write

$$\frac{d\alpha_i(t_k)}{dt} = \frac{\alpha_i(t_{k+1}) - \alpha_i(t_k)}{dt} \qquad (13)$$

For each of the snapshots in our data ensemble, we can now write an equation of the form (7) or (10), where the POD coefficient α_i and its derivative, $\frac{d\alpha_i}{dt}$, are known, and the model coefficients a_i , b_{ij} , and c_{ijk} are unknown. With *M* snapshots and *N* POD modes, we have a total of *MN* equations. Provided the number of snapshots *M* is sufficiently large, these equations can be solved in a least-squares sense in order to determine the model coefficients a_i , b_{ij} , and c_{ijk} .

III. Description and Results of The Test Application Problems

The test applications are chosen to demonstrate the ability of the method to obtain low-order models that are able to approximate different mathematical models of these test problems with a linear approximation.

A. The Heat Conduction Problem

The physical domain of the heat conduction problem in a 2D sheet is shown in Fig. 1 where the side AB is kept at constant temperature of 60°C and zero heat flux boundary conditions are imposed on the rest of the boundaries. The sheet is kept at room temperature of about 27°C initially.

Fig. 1. Physical domain for the heat diffusion problem.

While it is well known that the heat conduction problem can be modeled simply by

$$\frac{\partial T}{\partial t} = K\left(\frac{\partial^2 T}{\partial x^2} + \frac{\partial^2 T}{\partial y^2}\right) \qquad (14)$$

where $T(x, y, t)$ is the temperature and *K* is the thermal diffusivity of the material used for the sheet, for the purpose of this paper, the mathematical model is assumed to be unknown. A black-box solver takes in the diffusivity and initial conditions as inputs and yields the temperature data over the spatial grid for a specified time range and time step size. For these numerical experiments, we use a grid of size 6321 nodes. For a final time of up to 10 s with time step size of 0.5 s, the black-box solver yields 20 snapshots, which are used to obtain the POD modes. Three of the snapshots within this time range are presented in Fig. 2. One example material that we consider is gold, which has a diffusivity of 1.18 $cm^2\ s^{-1}$. Other types of materials are also tested in this paper with diffusivities of 0.85 $cm^2\ s^{-1}$ for SiC Al-MMC and 0.42 $cm^2\ s^{-1}$ for Al_20_3 Al-MMC [14].

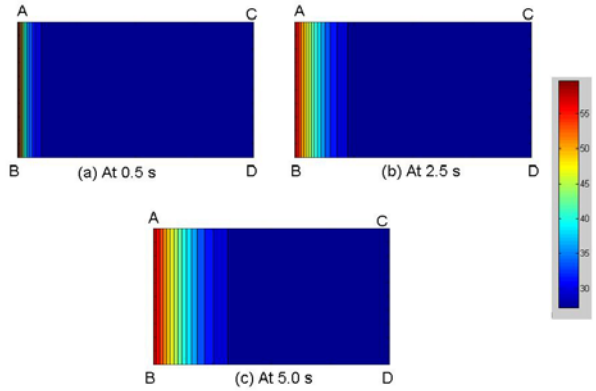

Fig. 2. The three snapshots of temperature at (a) 0.5 s, (b) 2.5 s, and (c) 5.0 s for K = 1.18 $cm^2\ s^{-1}$ with a maximum temperature of 60°C at AB.

Using the 20 snapshots obtained for the diffusivity of 1.18 $cm^2\ s^{-1}$, the POD modes are obtained. The relative energies of the POD modes, given by $\lambda_i / \sum_{j=1}^{M} \lambda_j$, are plotted in Fig. 3. It can be seen that by the sixth mode, the relative energies of the modes are less than 10^{-5}, indicating that their contributions to data in the snapshots set are less significant. Fig. 3 also shows that the 13th to the 20th POD modes have relative energies less than 10^{-15}, i.e. the eigenvalues of these modes are essentially zero. The first four POD modes of the heat conduction problem are presented in Fig. 4. Based on their relative energies shown in Fig. 3, these four POD modes represent a significant component of the snapshot data.

A linear approximation model as in (5) together with the POD modes is used derive the low-order approximate model. The values of the elements of the vectors and matrices of (7), a_i and b_{ij} , are computed by determining the POD modal coefficients for each of the snapshots using (12) and (13) and then solving the resulting least-squares system.

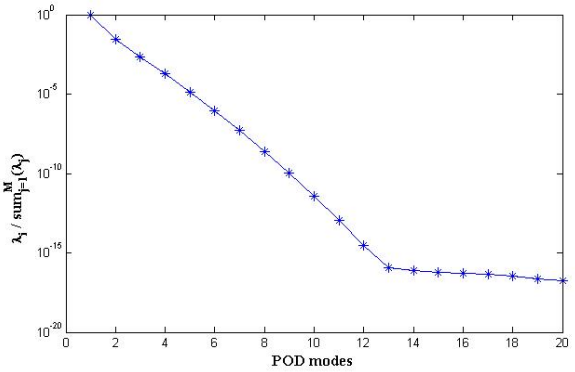

Fig. 3. The plot of relative energies of the POD modes for the heat conduction problem.

To ensure the stability of the low-order system, the eigenvalues of the low-order matrices should lie in the left half of the complex plane. As expected from Fig. 3, the maximum number of POD modes that can be used to yield a stable low-order system is N=12.

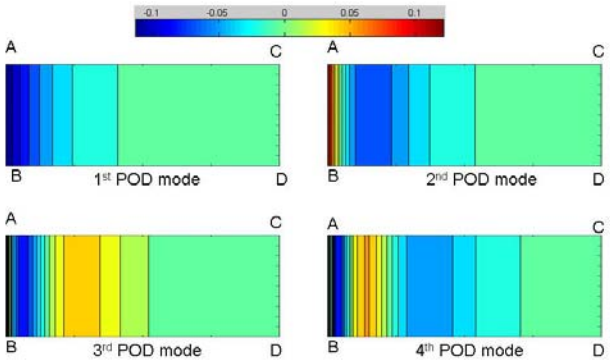

Fig. 4. The first four POD modes of the heat conduction problem for K = 1.18 cm^2 s^{-1}.

Fig. 5 and 6 show the plot of the coefficients of the first four POD modes using the original 20 ensemble snapshots, α_k, against time for the first fifty seconds of the metal sheet being heated. The red lines are the plots of the coefficients obtained by solving (12) based on the high-fidelity solutions. The approximate coefficients obtained from the low-order models of dimensions 4, 8, and 12 respectively are plotted in blue and compared to the coefficients from the high-fidelity solutions. One notes from Fig. 5 and 6 that while the coefficients for the first ten seconds of all the low dimensional models match those of the high-fidelity solutions, the coefficients of the last ten seconds in the plot show some differences.

The low-order model for N = 4, plotted using a blue + sign, show a marked difference from the coefficients shown in red in Fig. 6 for the last 20 seconds. The other two models of N=8 and N=12 yielded coefficients which are better matched to the coefficients of the high-fidelity solutions in red. The plots indicate that as the dimension of the low-order models increases, the accuracy of the solution increases too due to the inclusion of more POD modes.

TABLE I

THE MAXIMUM DIMENSION FOR THE LOW ORDER MODELS FOR VARIOUS MATERIALS TESTED AND THE RELATIVE ERROR OF THE PREDICTIONS OF THESE LOW ORDER MODELS AT TIME T = 50 SECONDS USING THEIR MAXIMUM DIMENSIONS.

Materials	Max N	$\frac{\|T(t=50)-T_N(t=50)\|}{\|T(t=50)\|}$
GOLD	12	0.034
SiC	12	0.035
Al-MMC		
Al_20_3	11	0.041
Al-MMC		

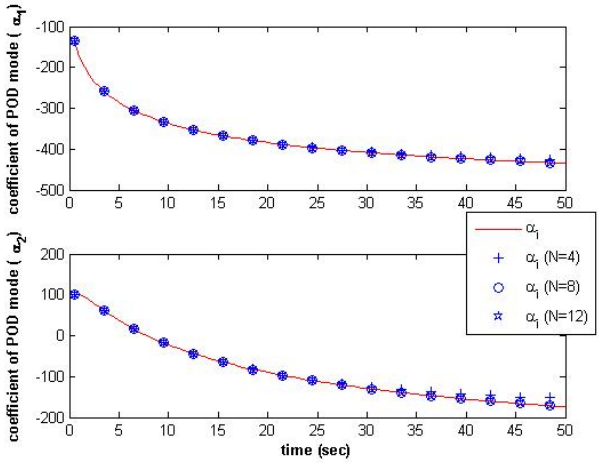

Fig. 5. The coefficients of the first two POD modes, α_1 and α_2, versus time. Red lines indicate the coefficients obtained from solving (10) using the high-fidelity computations for times beyond the snapshot range of the first ten seconds. The blue lines and icons are the approximate coefficients obtained from the low-order models for N = 4, 8, and 12.

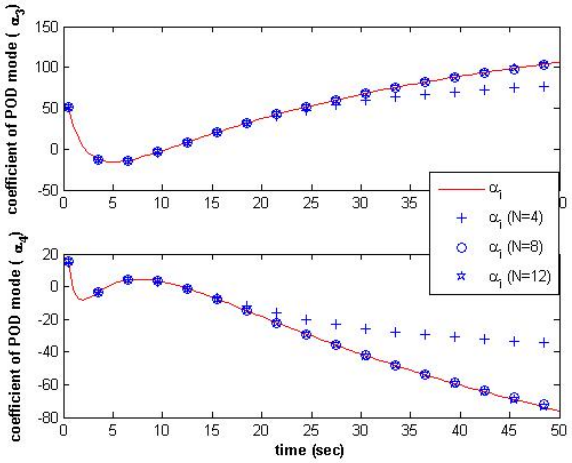

Fig. 6. The coefficients of the POD modes, α_3 and α_4, versus time. Red lines indicate the coefficients obtained from solving (12) using the high-fidelity computations for times beyond the snapshot range of the first ten seconds. The blue lines and icons are the approximate coefficients obtained from the low-order models for N = 4, 8, and 12.

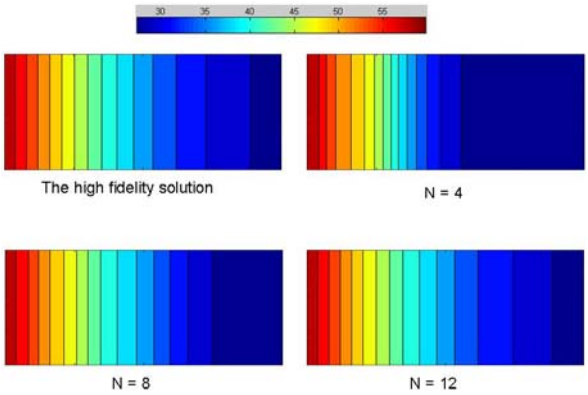

Fig. 7. The contour plots of the temperature from the high-fidelity/black-box solver and the low-order models at time = 40 seconds.

Fig. 7 shows the contour plots of the temperature at 40 seconds into the heating process obtained from the high-fidelity/black-box solver and the low-order models of dimensions 4, 8, and 12. One notes that the low-order model with N = 4 yields the least accurate temperature profile when compared to the high-fidelity solution while the low-order model with N = 12 yields the most accurate temperature profile. The results in Fig. 6 and 7 indicate the ability of the linear approximation to obtain low-order models that can predict the solutions of the heat conduction problem at times beyond the range used for the ensemble snapshots.

The other materials have also been tested using a snapshot ensemble of 20 for the given range of 10 seconds. The results are tabulated in Table 1. As in the case of the gold sheet, the silicon-aluminum compound, SiC Al-MMC, also allows for a low-dimensional model of N = 12 to approximate its heat conduction process while the aluminum oxide compound, Al_20_3 Al-MMC, allows for a low-dimensional model of N = 11. Even though only 10 seconds of information has been available for the low-order models, according to Table 1, they are able to predict the temperature profiles of the sheets within about 3 to 4% of the actual temperature profiles 40 seconds later.

B. The Contaminant Transport Problem

Contaminant transport problem [15] in a rectangular domain representing seepage of contaminants from the ground surface to deeper regions of the ground shown in Fig. 8 is considered next. In this problem, a leakage is assumed to occur from a processing plant, shown as a red block on the surface in Fig. 8. The leakage causes the contaminants to seep into the ground at a rate of 1 unit/day as indicated by the red lines in Fig. 8.There is constant groundwater flow in the direction of the arrows in Fig. 8, denoted by the groundwater velocity, v_x ,which advects the contaminants in the horizontal direction.

Fig. 8. Contaminant leak from a plant seeped through the ground and transported to other areas.

The contaminant transport problem can be represented by

$$\frac{\partial C}{\partial t} = D_x \frac{\partial^2 C}{\partial x^2} + D_z \frac{\partial^2 C}{\partial z^2} - v_x \frac{\partial C}{\partial x} \qquad (15)$$

where $C(x,z,t)$ is the contaminant concentration and D_x and D_z are the diffusivities in the horizontal and vertical directions. However, as in the heat conduction problem, the mathematical model is assumed to be unknown. A black-box solver receives the initial conditions, the diffusivities and the groundwater velocity, and outputs the concentration data for a specified time range and time step size. A grid size of 6321 nodes is used to process the solutions of contaminant concentration, which are used as snapshots for the POD modes. The initial condition for the problem is when the leakage first started, i.e. there is no contaminant in any other location in the ground besides the location of the processing plant itself.

Fig. 9 shows four of the 32 snapshots of contaminant concentration obtained within the first 8 days of the leakage for diffusivities of 0.5 m^2 day^{-1} and 0.05 m^2 day^{-1} in the horizontal and vertical directions and a groundwater velocity of 5 m/day. These 32 snapshots are used to obtain the POD modes.

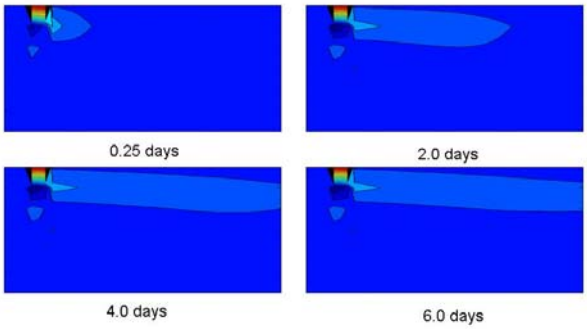

Fig. 9. The four snapshots within the range of the first 8 days of the contaminant leakage for diffusivities of 0.5 m^2 day^{-1} and 0.05 m^2 day^{-1} in the horizontal and vertical directions and a groundwater velocity of 4 m/day. The maximum contaminant concentration is 1 unit, shown in red, at the location of the processing plant.

The POD modes are computed from these 32 snapshots. The contour plots of the first four POD modes are shown in Fig. 10. These four modes have a combined energy of 99.87% of the total energy of the 32 POD modes.

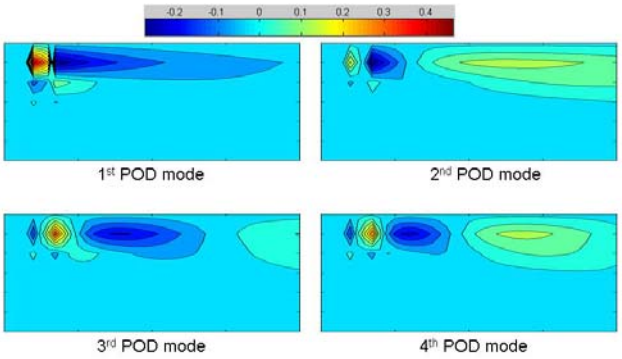

Fig. 10. Contour plots of the first four POD modes based on the 32 ensemble snapshots in Section III.

Linear low-order models of the form (7) are constructed computing the POD modal coefficients for each snapshot and solving the resulting least-squares system. In this case, the 32 snapshots allow for a low-order model with maximum dimension of N=16. Fig. 11 and 12 show the plot of the coefficients of the first four POD modes using the 32 snapshots, α_i, against time for the first 25 days of the leakage. The red lines are the plots of the coefficients obtained by solving (12) based on the high-fidelity solutions. The approximate coefficients obtained from the low-order models of dimensions 4, 8, and 16 respectively are plotted in blue and compared to the coefficients from the high-fidelity solutions. The results of all three low-order models are very similar to those of the high-fidelity/black-box solver. However, slight improvements to the accuracy of the predictions are observed in Fig. 12 as the dimensions of the low-order models increase.

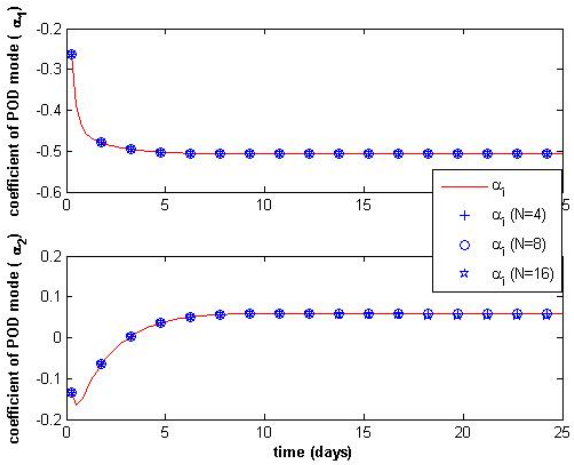

Fig. 11. The coefficients of the first two POD modes, α_1 and α_2, versus time. Red lines indicate the coefficients obtained from solving (12) using the high-fidelity computations for times beyond the snapshot range of the first ten seconds. The blue lines and icons are the approximate coefficients obtained from the low-order models for N = 4, 8, and 16.

TABLE II

THE MAXIMUM DIMENSION FOR THE LOW-ORDER MODELS FOR VARIOUS VELOCITIES TESTED AND THE RELATIVE ERROR OF THE PREDICTIONS OF THE CORRESPONDING LOW-ORDER MODELS ON THE 15TH AND 25TH DAY.

Velocity (m/day)	Max N	$\frac{\|C(t=15)-C_N(t=15)\|}{\|C(t=15)\|}$	$\frac{\|C(t=25)-C_N(t=25)\|}{\|C(t=25)\|}$
5	16	0.026	0.046
10	16	0.018	0.020
15	17	0.005	0.006
20	16	0.0001	0.0001

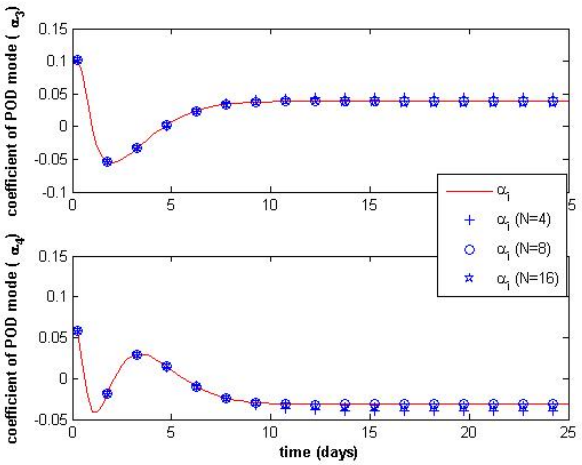

Fig. 12. The coefficients of the POD modes, α_3 and α_4, versus time. Red lines indicate the coefficients obtained from solving (12) using the high-fidelity computations for times beyond the snapshot range of the first ten seconds. The blue lines and icons are the approximate coefficients obtained from the low-order models for N = 4, 8, and 16.

Fig.13 shows the contour plots of the contaminant concentration in the ground on the 25th day of the leakage as obtained from the black-box solver and the low-order models with dimensions 4, 8 and 16. The plots look remarkably similar except for the trailing contaminant concentration. Both the low-order models of dimensions 4 and 8 under-predicted the spread of this trail in the vertical direction while the low-order model of dimension 16 managed to capture the spread of the trail in the vertical direction when compared to the high-fidelity solution. The prediction of the low-order model of dimension 16 on the 25th day is about 95.4% accurate while the prediction of the low-order models of dimensions 4 and 8 are about 94.1% and 94.6% accurate when compared to the high-fidelity solution.

Other tests with the same horizontal and vertical diffusivities but different groundwater velocities were also carried out; the results are tabulated in Table II. The relative errors of the predictions of the low-order models for these tests are less than 5%, giving assurance that the low-order models are able to predict the contaminant's movement on days beyond the range of the ensemble data. However, it could be observed from Table II that the relative errors of the predictions increase as the time increases beyond the range of the ensemble data, indicating that the low-order model may not be applicable for longer durations.

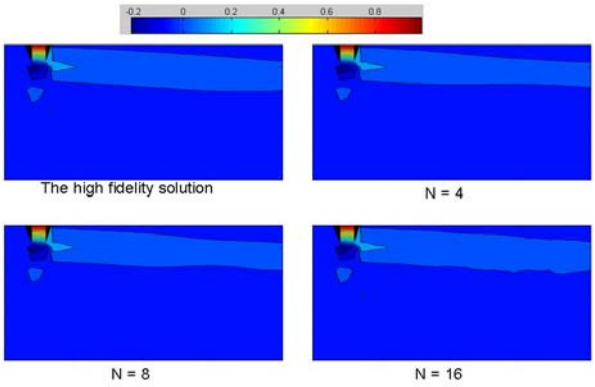

Fig. 13. The contour plots of the contaminant concentrations from the high-fidelity/black-box solver and the low-order models at time = 25 days.

IV. Conclusion

Based on the heat conduction and contaminant transport problems, the approximation method described in Section II has been successful in constructing low-order models for black-box linear applications with different actual mathematical models. The results showed that only a general knowledge of which approximation model to be used is necessary in the construction of the low-order models. As always with using the POD, having an appropriate quantity and range of snapshot data is very important for ensuring an accurate and stable low-order model.

Further tests are necessary to ensure that the black-box method is robust enough to tackle actual industrial problems whose mathematical models are more complex. As a first step, the quadratic approximation models should be tested on suitable applications.

Acknowledgment

The authors acknowledge the Singapore-MIT Alliance Computational Engineering Inter-University Research Program (IUP) for their support of this work.

References

[1] A.K. Noor and J.M. Peters, "Reduced basis technique for nonlinear analysis of structures." *AIAA Journal*, vol. 18, no. 4, pp. 455–462, 1980.

[2] J.P. Fink and W.C. Rheinboldt, "On the error behavior of the reduced basis technique for nonlinear finite element approximations." *Zeitschrift für Angewandte Mathematik und Mechanik*, vol. 63, no. 1, pp. 21–28, 1983.

[3] T.A. Porsching and M. Lin Lee, "The reduced basis method for initial value problems," *SIAM Journal on Numerical Analysis*, vol. 24, no. 6, pp. 1277–1287, 1987.

[4] P. Feldmann and R.W. Freund, "Efficient linear circuit analysis by Pade approximation via the Lanczos process," *IEEE Transactions on Computer-Aided Design of Integrated Circuits and Systems*, vol. 14, no. 5, pp. 639-649, 1995.

[5] R.W. Freund and P. Feldmann, "Reduced-order modeling of large passive linear circuits by means of the SyPVL algorithm," in *Proceedings of the 1996 IEEE/ACM International Conference on Computer-Aided Design*, pp. 280-287, 1996.

[6] K. Gallivan, E. Grimme, and P. Van Dooren, "Asymptotic waveform evaluation via a Lanczos method," *Applied Mathematics Letters*, vol. 7, no. 5, pp. 77-80, 1994.

[7] J.L. Lumley, "The structure of inhomogeneous turbulence," in *Atmospheric Turbulence and Wave Propagation*, Yaglom and V.I. Tatarski (eds). Nauka, Moscow, pp. 166-178, 1967.

[8] L. Sirovich and M. Kirby, "Low dimensional procedure for the characterization of human faces," *Journal of the Optical Society of America A*, vol. 4, no. 3, pp. 519-524, 1987.

[9] L. Sirovich, "Turbulence and the dynamics of coherent structures, parts I-III" *Quarterly of Applied Mathematics*, vol. 65, pp. 561-590, 1987.

[10] H.V. Ly and H.T. Tran, "Modeling and Control of Physical Processes Using Proper Orthogonal Decomposition," *Mathematical and Computer Modelling*, vol. 33, pp. 223-236, 2001.

[11] E. Caraballo, X. Yuan, J. Little, M. Debiasi, P. Yan, A. Serrani, J. H. Myatt, and M. Samimy, "Feedback Control of Cavity Flow Using Experimental Based Reduced Order Model," in *35th AIAA Fluid Dynamics Conference and Exhibit*, AIAA 2005-5269, 6-9 June 2005, Ontario, Canada.

[12] G. Berkooz, P. Holmes, and J.L. Lumley, "The proper orthogonal decomposition in the analysis of turbulent flows," *Annual Reviews Fluid Mechanics*, vol. 25, pp. 539-575, 1993.

[13] A.Bjorck, *Numerical Methods for Least Squares*, SIAM, Philadelphia 1996, ch. 4.

[14] R. L. Hecht, R. B. Dinwiddie, W. D. Porter, and H. Wang, *Thermal transport properties of aluminum metal matrix composites for brake applications*, 1999. [Online] Available: http://www.html.ornl.gov/tpuc/brakes.html

[15] C. Zheng and G.D. Bennett, Applied Contaminant Transport Modeling: Theory and Practice. *International Thomson Publishing Inc.*, 1995.